Polymer Nanotube Membranes Synthesised via Liquid Deposition in Anodic Alumina

Zheyi Meng [a], Serena Casanova [b], Halan Mohamed [a], Nidhi Kapil [a], Xiao Xiao [c], Yuheng Zhang [d], Marc-Olivier Coppens [a, *], Davide Mattia [b, *]

a. EPSRC ''Frontier Engineering'' Centre for Nature-Inspired Engineering & Department of Chemical Engineering, University College London, London, WC1E 7JE, UK.

b. Department of Chemical Engineering and Centre for Advanced Separations Engineering, University of Bath, Bath, BA2 7AY, UK.

c. School of Material Science and Engineering, Beihang University, Beijing, 100191, China.

d. School of Chemistry, Beihang University, Beijing, 100191, China.

* Corresponding author: d.mattia@bath.ac.uk, m.coppens@ucl.ac.uk

Graphical abstract

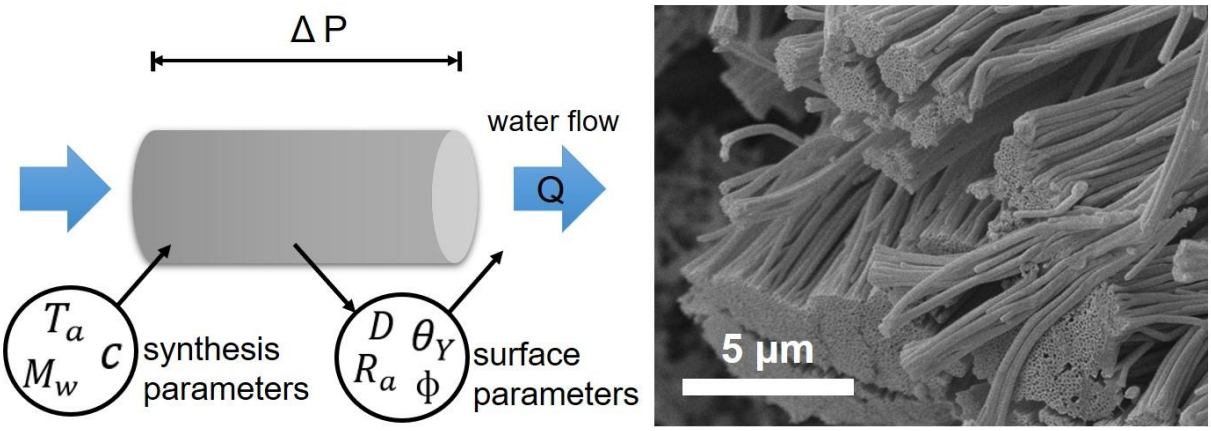

Polymer Nanotube Membranes Synthesised via Liquid Deposition in Anodic Alumina

Abstract

Self-standing polystyrene nanotube (PNT) membranes have been fabricated from liquid deposition in the pores of anodic alumina. PNTs were deposited using 3 wt% concentration of 90 kDa polystyrene in the starting solution, followed by 2 h annealing in Argon. Initial polymer concentration, polymer molecular weight and annealing time were varied, and their impact on water flow through the nanotubes assessed. These results open the way to creating PNT membranes with well-defined pores of low tortuosity and tuneable surface properties, overcoming the limits of current polymeric membranes, whose internal transport pathway cannot be controlled or defined as well as for the case of the PNTs presented here.

Keywords

Polymer nanotube, anodic alumina membrane, liquid deposition, water flow enhancement

Polymeric membranes are used in large-scale separation processes, from seawater desalination to CO_2 capture and the purification of drugs and chemicals [1]. However, fundamental problems to further improving these membranes remain, such as fouling, selectivity and stability, primarily related to constraints on the types of polymers and the micro-structures that can be obtained with current manufacturing methods [2], including phase inversion, interfacial polymerization, track etching, and sintering [3]. Polymeric membranes can be broadly classified according to their pore size, from ultrafiltration (UF) membranes, which have an irregular, highly tortuous porous structure [4], to nanofiltration and reverse osmosis membranes, which have a dense structure, without well-defined pores, and in which transport occurs via the solution-diffusion model in the free volume between the polymer chains [5]. In all instances, these limitations result in increased transport resistance, which, in turn, requires more energy to force the liquid through the membrane [6]. Considerable efforts to control the structure of transport pathways in polymeric membranes have been made over the years, with work ranging from copolymer self-assembly into isoporous membranes [7], to mimicking water channels found in biological membranes, such as aquaporins [8].

While these methods allow for fine control over pore size and tortuosity [9], they have not yet been able to obtain regular, cylindrical pores via a process with potential for scale-up [10]. The first results showing a high water flow rate in carbon nanotubes (CNTs) not only promised higher performance compared to current polymeric membranes, but also provided a well-defined and tuneable transport pathway ranging from ultrafiltration to reverse osmosis [11, 12]. The former aspect was due to the low frictional losses associated with water flow through the tubes and related to the unfavourable energetic interaction between water and the sp2 graphitic structure of the CNTs [13, 14]. The effect of this interaction on the flow can be quantified via the concept of a slip length, λ, as a generalisation of the Hagen-Poiseuille equation for flow in a single pore:

$$q = \frac{\pi D^4 \Delta P}{128\,\mu L \tau}\left(1 + \frac{8\lambda}{D}\right) \quad (1)$$

where q is the volumetric flow rate through a single pore of diameter D and length L, ΔP is the applied pressure difference, μ is the fluid viscosity, and τ is the pore's tortuosity, i.e. the deviation from a straight pore connecting a membrane's feed and permeate side. For anodic alumina membranes $\tau \sim 1$, with all pores aligned perpendicularly to the membrane's surface [11]. Hence, the membrane's volumetric flow rate $Q = nq$, where n is the number of pores, linked to a membrane's porosity by the following equation:

$$\phi = \frac{1}{A_{mem}} \sum_{i=1}^{n} \frac{\pi D_i^2}{4} \quad (2)$$

where A_{mem} is the area of the membrane. When the pore size distribution is narrow, as in the case of anodic alumina, the porosity can be taken as $\phi \sim \frac{n\pi D^2}{4A_{mem}}$, with the resulting flow rate equal to [11]:

$$Q = \frac{\phi\, A_{mem} D^2 \Delta P}{32\,\mu L \tau}\left(1 + \frac{8\lambda}{D}\right) \quad (3)$$

For membranes, a more useful quantity to report is the permeance, defined as follows:

$$K = \frac{Q}{A_{mem} \Delta P} \quad (4)$$

with units of L $m^{-2}h^{-1}bar^{-1}$. A measure of the increase in K_{exp}, the experimental permeance due to slip, compared to $K_{\lambda=0}$, the no slip case, is termed flow enhancement [1]:

$$\varepsilon = \frac{K_{exp}}{K_{\lambda=0}} = 1 + \frac{8\lambda}{D} \quad (5)$$

Values of ε as high as 10^5 were measured experimentally and predicted via molecular dynamics simulations for carbon nanotubes [12]. Furthermore, CNT array membranes had tortuosity values, $\tau \sim 1$, compared to 2-5 for commercial UF membranes [15]. Unfortunately, the challenge of aligning carbon nanotubes in the polymeric matrix and the need to functionalise the nanotubes to obtain good adhesion with polymeric matrices are hindering translation from the lab to practical use [16, 17]. Transport studies in CNTs also showed that tuning the surface

chemistry and structure of the nanotubes, e.g. to achieve separation selectivity, can have a significant effect on water flow, with a range of different nanotube materials tested so far [11, 18, 19].

Here, a fundamentally novel approach is proposed, creating straight (τ~1), cylindrical, polystyrene nanotubes, marrying the advantages of using a commonly used polymer with the formation of a well-defined and tuneable permeation pathway provided by the nanotubes. In this work, the synthesis of polystyrene nanotubes (PNTs) is performed from liquid deposition inside the pores of anodic alumina (AAMs) templates, resulting in the formation of polymer nanotube (PNT) membranes (Fig. 1a). AAMs were soaked into 3-5 ml of chloroform solution with PS (90 or 200 kDa) for an hour at 40 °C in concentrations of 1, 3 and 7 wt%, and then dried in air on a stainless-steel support. The samples were then annealed at 220 °C for 2 or 12 hours in a tubular furnace with a protective argon flow of 600 mL/min. After synthesis, all membranes were etched by oxygen plasma. Further details about the synthesis and characterisation of the membranes produced can be found in the supplementary information document.

All membranes appeared opaque and faintly yellow after synthesis, as shown in Fig. 1b, and their top and bottom surface appeared clear of debris (Fig. 2). Via FESEM, plasma etching on the PNT membranes synthesis was optimised to a duration of 5 min for the baseline sample (3 wt%, 90 kDa, 2 h), which was found to be enough to totally remove the polymer debris from the membrane's top and bottom surfaces in the baseline sample (Fig. S1).

SEM cross-section micrographs show the PNTs released from the template and forming along the whole thickness of the anodic alumina template (Fig. 3). An increase in the polymer molecular weight leads to the formation of more fragmented nanotube walls (Fig. 3d) with increased roughness (Fig. 3d1). This was attributed to the fact that the PS with lower molecular weight has a lower glass transition temperature of 106 °C (Fig. S2) with better adherence to the substrate, compared to 111 °C for the higher molecular weight PS [20], and resulting in a more

uniform PNT structure under the same annealing condition. The annealing temperature was fixed at 220 °C, as this is well above the polymer glass transition temperature of 106-111 °C in all cases. SEM analysis shows that a change in annealing time does not significantly impact the tubes' length (Fig. 3e). The average pore size for the anodic alumina and the PNT membranes is reported in Table 1. The value for the anodic alumina (200 ± 8 nm) is consistent with diameters reported in the literature for the same templates [21]. The values reported for the PNT membranes, the result of 3 measurements on each membrane, show very narrow size distributions (Fig. 4), consistent with the formation of a uniform polymer coating inside the pores of the anodic alumina. Such uniform coating was also observed via TEM (Fig.3), further confirming the hollow nature of the PNTs [22]. It is noted here that the diameters of the PNTs in the TEM appear significantly larger than those measured by porometry. This is attributed to the fact that the PNTs, with relatively large diameters and thin walls, tend to flatten once placed onto the TEM grid, in analogy to what has been previously observed for large carbon nanotubes (or nanopipes) synthesized in the pores of 200 nm diameter anodic alumina [21].

The produced PNT membranes were tested for pure water flow in the previously described, customised dead-end filtration setup with effective diameter of 10 mm [13]. The experimental permeance, K_{EXP}, was calculated from measurements on three membrane samples for each set of synthesis parameters. The experimental permeance values obtained here are comparable with those of commercial UF membranes [15]. However, a direct comparison with PS membranes is not possible, as these are generally used for membrane distillation or ion exchange, rather than water permeance [2]. An indirect comparison with an ultrafiltration PS-PEO membrane [23] shows an increase of ~40% in permeance for the 3 wt% PS (90 kDa). The theoretical value for permeance (K_{HP}) can be calculated using Eq. 4 by inserting the value of Q obtained from Eq. 3 for $\lambda = 0$, computed using the average diameter measured by porometry for each nanotube membrane (Table 1).

1 wt% of PS (90 kDa) in the starting solution was enough to reduce the pore diameter from 200 nm (AAM template) to 95 nm (PNTs). A further increase in the concentration to 3 wt% (the baseline) led to a pore diameter of 45 nm. A further increase in concentration to 7 wt% did not produce any further reduction in pore size, possibly due to pore clogging and thicker tubes (Fig. 3c1 & 3c2). The water Young contact angle (θ_Y), computed using the Cassie-Baxter model for porous surfaces (Eq. 6), increases with increasing PS concentration from $65 \pm 2^{\mathbf{o}}$ to $116 \pm 2^{\mathbf{o}}$ (Table 1). The low contact angle for the lowest PS concentration is attributed to potentially incomplete coverage of the AAM's surface by the polymer.

As the polymer coats the walls of the AAM, both porosity and permeance are reduced (Table 1), as expected [11]. However, the flow enhancement, ε, increases, with a maximum of 4.3x for a starting PS concentration of 3 wt%, indicating somewhat more "slippery" PNTs. This modest increase can be attributed to the increased hydrophobicity of the PS tubes compared to the AAM (viz. contact angles in Table 1), in analogy to what is observed for other nanotube materials, where an increase in hydrophobicity resulted in an increase in slip and, hence, flow enhancement [13]. Compared to the optimised concentration of 3 wt%, higher and lower PS concentrations result in lower or even no flow enhancement. For Sample b (1 wt%) in Table 1, as analysed above, the incomplete polymer coverage of the substrate leads to an increased roughness of the PNTs, which is reflected in the measured contact angle. For Sample c (7 wt%), the excessive polymer causes pore clogging and thicker coverage in the substrate, resulting in the low water flux noted in Table 1. Using a higher molecular weight PS (200 kDa) in the 3 wt% starting solution did not change the contact angle (Table 1) compared to the 90 kDa PS at the same concentration, but it resulted in a significantly lower flow enhancement. This difference is attributed to the less regular structure of the polymer nanotubes produced using the 200 kDa PS than the 90 kDa PS (cf. Fig. 3a with Fig. 3d), which increases the resistance to flow along the tubes. Such less regular structure of the PNTs is attributed to an increase in Rayleigh instabilities during film formation with higher molecular weights [24]. An increase in

annealing time from 2 to 12 h did not produce any significant effect on the flow enhancement, despite a small increase in contact angle, attributed to chain rearrangement in the polystyrene [24]. It is noted that the increases in flow enhancement are used here primarily as a measure of the changes induced by the polymer coating. In fact, the flow enhancement in PNTs are modest compared to those observed in cylindrical nanopores of track etched polymeric membranes (Table S1) [25]. However, the high porosity (20-30%) endows the PNT-AAMs with comparable or even better water permeance to track etched membranes, where the porosity is at least an order of magnitude lower. Thus, the PNTs have good prospects in filtrations and separations, and the trade-off between membrane porosity and flow enhancement of a single nanopore to increase the overall flow should be investigated in future work.

In summary, the formation of straight ($\tau \sim 1$) polystyrene nanotube membranes via soaking of anodic alumina membranes in polystyrene solutions is reported here for the first time. The effect of polystyrene concentration, molecular weight and annealing time on the structure of polystyrene nanotubes and on the pure water permeance through the membranes was investigated, showing that a flow enhancement of 4.3x the bare anodic alumina case was obtained for a 3 wt% concentration of 90 kDa polystyrene in the starting solution, followed by 2 h annealing in Argon. Further increases in initial polymer concentration, polymer molecular weight and annealing time did not produce any significant increase in pure water permeance. These results open the way to creating polymeric nanotube membranes with low-tortuosity, well-defined pore structure and tuneable surface properties, overcoming the limits of current polymeric membranes whose internal transport pathway cannot be controlled or defined as well as for the case of the polymer nanotubes presented here.

Acknowledgements

The authors gratefully acknowledge support from the Engineering and Physical Sciences Research Council (EPSRC) for a “Frontier Engineering” grant supporting the Centre for Nature

Inspired Engineering (EP/K038656/1), grant EP/M01486X/1 (SynFabFun) and Doctoral Training Award (534372). Yuanhang Global Study Summer Research Program funding from Beihang University is also acknowledged for their financial support.

References

[1] H.B. Park, J. Kamcev, L.M. Robeson, M. Elimelech, B.D. Freeman, Science, 356 (2017) eaab0530.

[2] M. Radjabian, V. Abetz, Prog. Polym. Sci., 102 (2020) 101219.

[3] X. Tan, D. Rodrigue, Polymers, 11 (2019) 1160.

[4] B. Van der Bruggen, C. Vandecasteele, T. Van Gestel, W. Doyen, R. Leysen, Environ. Prog. Sustain., 22 (2003) 46-56.

[5] K.P. Lee, T.C. Arnot, D. Mattia, J. Membr. Sci., 370 (2011) 1-22.

[6] M. Mulder, Basic principles of membrane technology, Springer Science & Business Media, 2012.

[7] K.-V. Peinemann, V. Abetz, P.F. Simon, Nat. Mater., 6 (2007) 992-996.

[8] S. Gravelle, L. Joly, F. Detcheverry, C. Ybert, C. Cottin-Bizonne, L. Bocquet, Proc. Natl. Acad. Sci. U.S.A., 110 (2013) 16367-16372.

[9] J.I. Clodt, V. Filiz, S. Rangou, K. Buhr, C. Abetz, D. Höche, J. Hahn, A. Jung, V. Abetz, Adv. Funct. Mater., 23 (2013) 731-738.

[10] T. Bucher, V. Filiz, C. Abetz, V. Abetz, Membranes, 8 (2018) 57.

[11] D. Mattia, H. Leese, K.P. Lee, J. Membr. Sci., 475 (2015) 266-272.

[12] M. Majumder, N. Chopra, R. Andrews, B.J. Hinds, Nature, 438 (2005) 44-44.

[13] S. Casanova, M.K. Borg, Y.J. Chew, D. Mattia, ACS Appl. Mater. Interfaces, 11 (2018) 1689-1698.

[14] E. Secchi, S. Marbach, A. Niguès, D. Stein, A. Siria, L. Bocquet, Nature, 537 (2016) 210-213.

[15] M. Cheryan, Ultrafiltration and microfiltration handbook, CRC press, 1998.

[16] H. Zhao, S. Qiu, L. Wu, L. Zhang, H. Chen, C. Gao, J. Membr. Sci., 450 (2014) 249-256.

[17] B. Corry, Energy Environ. Sci., 4 (2011) 751-759.

[18] K.P. Lee, H. Leese, D. Mattia, Nanoscale, 4 (2012) 2621-2627.

[19] M. Bechelany, S. Bernard, A. Brioude, D. Cornu, P. Stadelmann, C. Charcosset, K. Fiaty, P. Miele, J. Phys. Chem. C, 111 (2007) 13378-13384.

[20] M. Zhang, P. Dobriyal, J.-T. Chen, T.P. Russell, J. Olmo, A. Merry, Nano Lett., 6 (2006) 1075-1079.

[21] M.P. Rossi, Y. Gogotsi, K.G. Kornev, Langmuir, 25 (2009) 2804-2810.

[22] S. Schlitt, A. Greiner, J.H. Wendorff, Macromolecules, 41 (2008) 3228-3234.

[23] H. Yang, Z. Wang, Q. Lan, Y. Wang, J. Membr. Sci., 542 (2017) 226-232.

[24] G. Matsuba, K. Kaji, K. Nishida, T. Kanaya, M. Imai, Macromolecules, 32 (1999) 8932-8937.

[25] K.J. Kim, P.V. Stevens, J. Membr. Sci., 123 (1997) 303-314.

Table 1. Average pore size (D), porosity (ϕ), theoretical permeance ($K_{\lambda=0}$), experimental permeance (K_{exp}), flow enhancement (ε), and Young contact angle computed using the Cassie-Baxter equation (θ_Y).

Sample	D (nm)	ϕ (-)	$K_{\lambda=0}$ (L m^{-2} h^{-1} bar^{-1})	K_{exp} (L m^{-2} h^{-1} bar^{-1})	ε (-)	θ_Y (°)
AAM	200 ± 8	0.35	3539	4210 ± 250	1.2 ± 0.1	41 ± 2
a (3 wt%, 90 KDa, 2h)	45 ± 1	0.23	119	513 ± 45	4.3 ± 0.4	105 ± 2
b (1 wt%, 90 KDa, 2h)	95 ± 2	0.38	865	2040 ± 240	2.4 ± 0.3	65 ± 2
c (7 wt%, 90 KDa, 2h)	49 ± 1	0.29	176	97 ± 33	0.6 ± 0.2	116 ± 2
d (3 wt%, 200 KDa, 2h)	46 ± 1	0.31	164	282 ± 76	1.7 ± 0.5	108 ± 2
e (3 wt%, 90 KDa, 12 h)	53 ± 1	0.25	180	692 ± 33	3.9 ± 0.2	114 ± 2

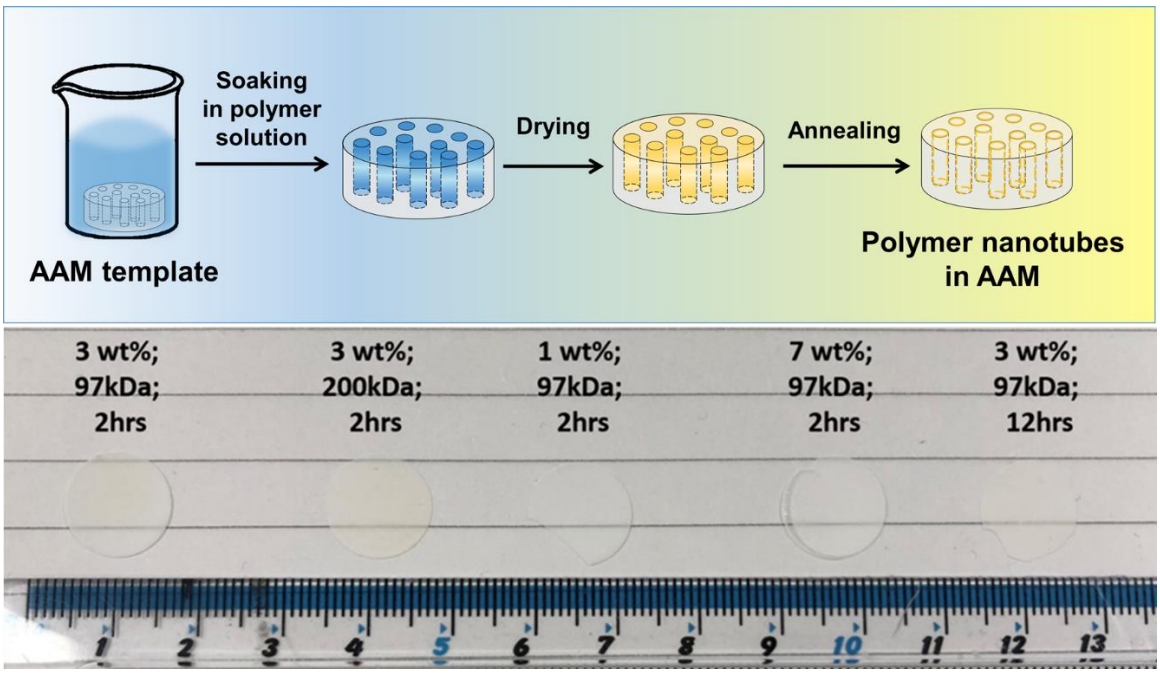

Fig. 1. Schematic of the synthesis of PNT-AAMs via soaking method (top); pictures of the PNT-AAMs under investigation in this work (bottom).

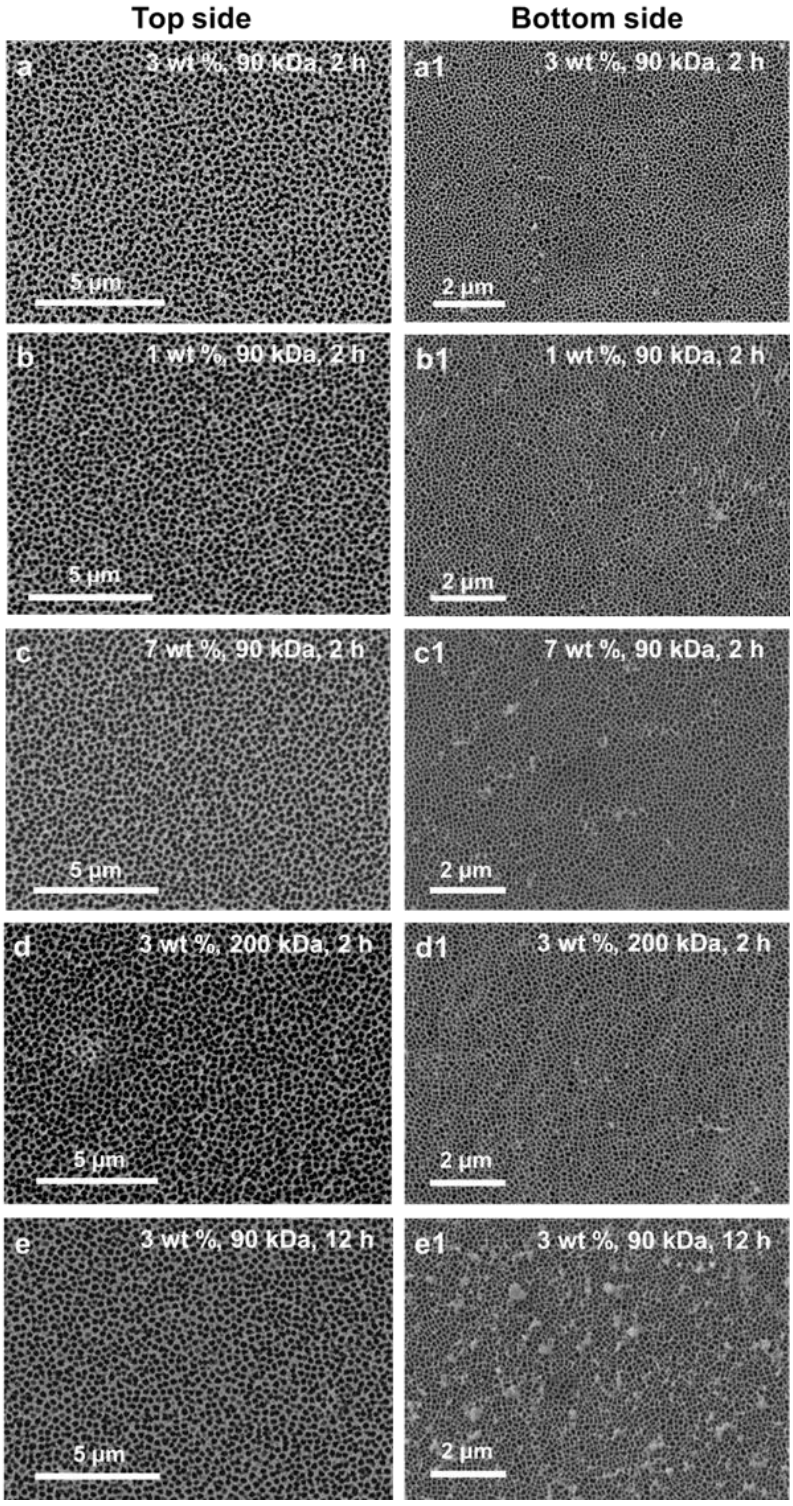

Fig. 2. Top (left) and bottom (right) surfaces for (a, a1) 3 wt%, 90 kDa, 2 h; (b, b1) 1 wt%, 90 kDa, 2 h; (c, c1) 7 wt%, 90 kDa, 2 h; (d, d1) 3 wt%, 200 kDa, 2 h; (e, e1) 3 wt%, 90 kDa, 12 h, respectively. Top sides are taken at x5,000 magnification. Bottom sides are taken at x10,000 magnification.

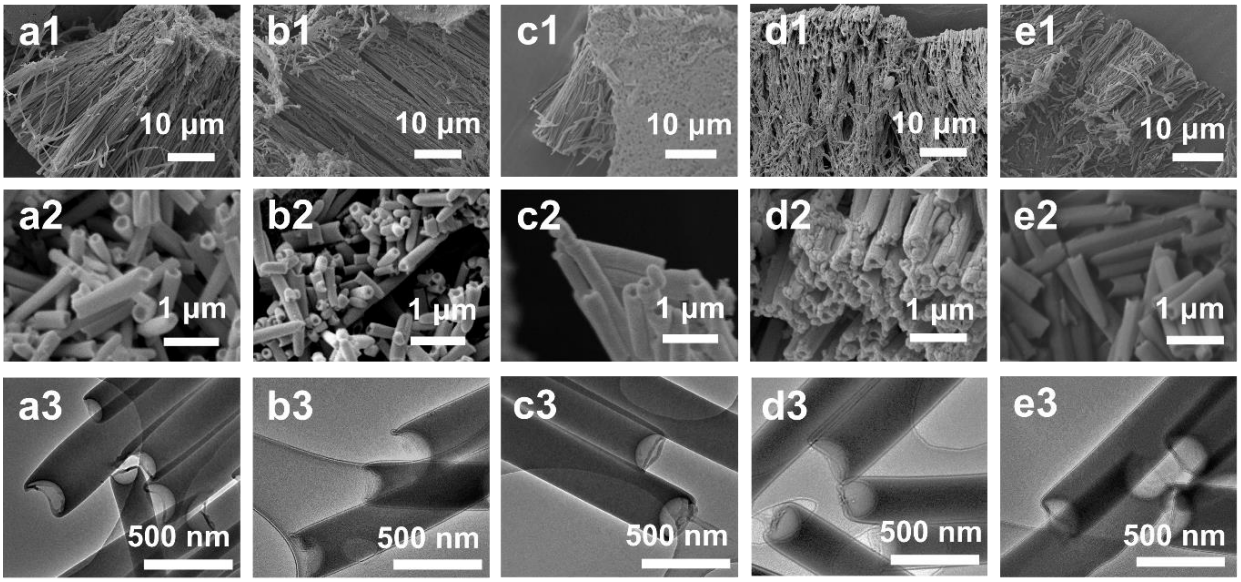

Fig. 3. SEM micrographs of polystyrene PNTs with different PS concentration, molecular weight and annealing time. Cross-section views (x2,000 magnification) and opening views (x25,000 magnification): (a1 & a2) 3 wt%, 90 kDa, 2 h (baseline); (b1 & b2) 1 wt%, 90 kDa, 2 h; (c1 &c2) 7 wt%, 90 kDa, 2 h; (d1 & d2) 3 wt%, 200 kDa, 2 h; (e1 & e2) 3 wt%, 90 kDa, 12 h. TEM micrographs of PNTs prepared with different PS concentration, molecular weight and annealing time: (a3) 3 wt%, 90 kDa, 2 h (baseline); (b3) 1 wt%, 90 kDa, 2 h; (c3) 7 wt%, 90 kDa, 2 h; (d3) 3 wt%, 200 kDa, 2 h; (e3) 3 wt%, 90 kDa, 12 h, respectively.

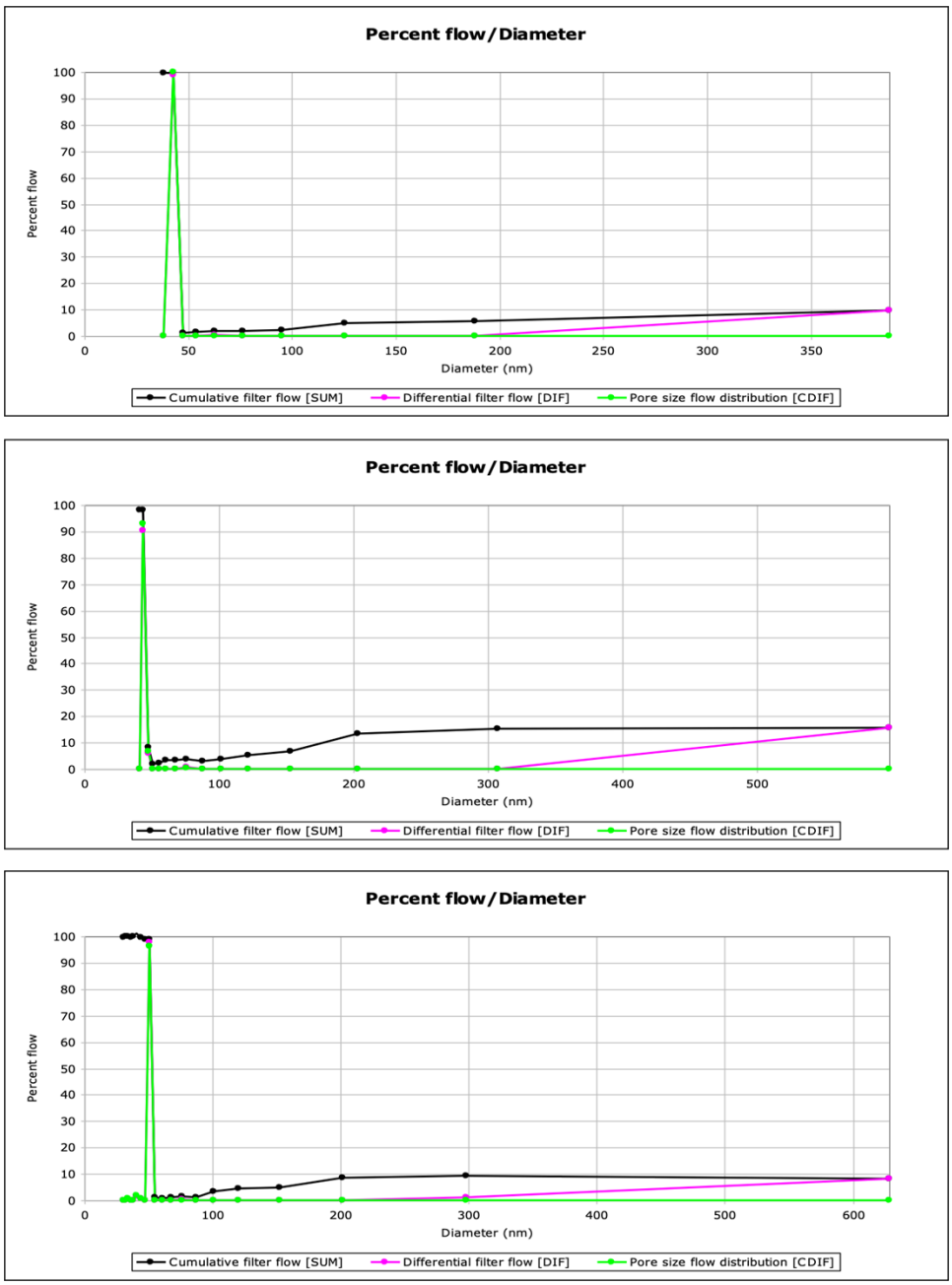

Fig. 4. Selected pore size distributions for 3wt% samples: (top) 90 kDa, 2h; (middle) 200 kDa, 2h; (bottom) 90 kDa, 12h.

CRediT author statement

Zheyi Meng: Methodology, Validation, Investigation, Formal analysis, Visualization, Writing – Original Draft, Project administration. **Serena Casanova**: Methodology, Validation, Investigation, Visualization, Writing – Original Draft. **Halan Mohamed**: Methodology, Investigation, Writing – Original Draft. **Nidhi Kapil**: Investigation, Writing – Original Draft. **Xiao Xiao**: Investigation. **Yuheng Zhang**: Investigation. **Marc-Olivier Coppens**: Conceptualization, Formal analysis, Resources, Writing – Review & Editing, Supervision, Project administration, Funding acquisition. **Davide Mattia**: Conceptualization, Formal analysis, Resources, Writing – Review & Editing, Supervision, Project administration, Funding acquisition